White light emission of Eu^{3+}-based hybrid xerogels

L. D. Carlos* and R. A. Sá Ferreira
Departamento de Física, Universidade de Aveiro, 3810 Aveiro, Portugal

V. De Zea Bermudez
Secção de Química, Universidade de Trás-os Montes e Alto Douro, Quinta de Prados, Apartado 202, 5001 Vila Real Codex, Portugal

Celso Molina, Luciano A. Bueno, and Sidney J. L. Ribeiro
Instituto de Química–UNESP, CP 355, 14801-970, Araraquara SP, Brazil

(Received 23 March 1999)

The luminescence spectra and extended x-ray-absorption fine-structure (EXAFS) measurements of a series of Eu^{3+}-based organic/inorganic xerogels were reported and related to the local coordination of the lanthanide cations. The hybrid matrix of these organically modified silicates, classed as $U(2000)$ ureasils, is a siliceous network to which short organic chains containing oxyethylene units are covalently grafted by means of urea bridges. The luminescent centers were incorporated as europium triflate, $Eu(CF_3SO_3)_3$, and europium bromide, $EuBr_3$, with concentrations $200 \geqslant n \geqslant 20$ and $n=80$, 40, and 30, respectively—where n is the number of ether oxygens in the polymer chains per Eu^{3+} cation. EXAFS measurements were carried out in some of the $U(2000)_nEu(CF_3SO_3)_3$ xerogels ($n=200$, 80, 60, and 40). The obtained coordination numbers N ranging from 12.8, $n=200$, to 9.7, $n=40$, whereas the average Eu^{3+} first neighbors distance R is 2.48–2.49 Å. The emission spectra of these multiwavelength phosphors superpose a broad green-blue band to a series of yellow-red narrow $^5D_0 \rightarrow {}^7F_{0-4}$ Eu^{3+} lines and to the eye the hybrids appeared to be white, even at room temperature. The ability to tune the emission of the xerogels to colors across the chromaticity diagram is achieved by changing the excitation wavelength and the amount of salt incorporated in the hybrid host. The local environment of Eu^{3+} is described as a continuous distribution of closely similar low-symmetry network sites. The cations are coordinated by the carbonyl groups of the urea moieties, water molecules, and, for $U(2000)_nEu(CF_3SO_3)_3$, by the SO_3 end groups of the triflate anions. No spectral evidences have been found for the coordination by the ether oxygens of the polyether chains. A mean radius for the first coordination shell of Eu^{3+} is calculated on the basis of the emission energy assignments. The results obtained for $U(2000)_nEu(CF_3SO_3)_3$, 2.4 Å for $90 \geqslant n \geqslant 40$ and 2.6 and 2.5 Å for $n=30$ and 20, respectively, are in good agreement with the values calculated from EXAFS measurements. The energy of the intraconfigurational charge-transfer transitions, the redshift of the $^5D_0 \rightarrow {}^7F_0$ line, with respect to the value calculated for gaseous Eu^{3+}, and the hypersensitive ratio between the $^5D_0 \rightarrow {}^7F_2$ and $^5D_0 \rightarrow {}^7F_1$ transitions, point out a rather low covalency nature of the Eu^{3+} first coordination shell in these xerogels, comparing to the case of analogous polymer electrolytes modified by europium bromide. [S0163-1829(99)03138-0]

I. INTRODUCTION

Solid thin polymer ion conductor films involving complexes of macromolecules and various ionic salts, i.e., polymer electrolytes, have been the focus of considerable scientific interest during the last two decades.[1–3] The main driving force in this research was initially originated by the possibility of using these materials, essentially incorporating monovalent lithium salts in poly(oxyethylene), POE, in a variety of electrochemical and electrochromic displays, such as rechargeable high-energy-density batteries, proton exchange polymer electrolytes, membrane fuel cells, and variable-transmission ''smart'' windows.[1–3]

In spite of the tremendous quantity of physical and chemical characterization measurements carried out during the last 20 years, progress on the understanding of the microscopic dynamics and ionic transport features of these materials have been severely restricted by the lack of structural data. In fact, only very recently was substantial progress in the analysis of the x-ray-diffraction patterns of salt-rich polymer electrolytes reported.[4] The difficulties encountered in determining their crystal structures by single-crystal methods were, thus, solved and, consequently, the crystal structure of some polymer-in-salt complexes have been established.[4] However, regarding the amorphous regions of polymer electrolytes in which the charge transport processes predominantly occur,[1–3] both the local interactions between the ions and the polymer chains and the local polymer segmental motions—which are critical for long-range charge transport—are poorly known. Both vibrational and electronic spectroscopic techniques are relevant tools for gaining some insight about the structural molecular characteristics of those amorphous regions. These techniques have been frequently used in various polymer-salt complexes to investigate several aspects of their molecular characteristics, such as, for instance, the conformation of the polymer chains,[5–7] the anionic and cationic environments,[8–24] the vibrational modes of polymer-cation coordination,[9–11,24] and ether oxygen-metal ion stretching motions.[10,11,22]

In the case of polymer electrolytes incorporating lan-

thanide salts, since the first initial reports indicating that trivalent cations were also soluble in POE and poly(oxypropylene), POP,[13,14] several papers have been published during this decade showing that the ion-polymer chain interactions can be investigated using the cation emission features,[14–24] and the active vibrational modes of the anions.[6,8–12,22,24] In particular, for POE electrolytes incorporating $EuBr_3$ the observed emission energies have previously been used for determining the average Eu^{3+} nearest ligands distance,[16,19] the associated local symmetry group,[15,19] and the number of nearest oxygens.[23] Moreover, for these europium-based polymer electrolytes a structural model of chains of interacting coordination shells (characterized by the luminescent center and by its nearest ligands oxygens) was derived, allowing the determination of the interaction energy between adjacent coordination shells.[23]

The narrow room-temperature luminescence characteristic of this encapsulation of lanthanide centers into the oxygen-lined helical turns of POE combined with the advantages of processable ionically plastic films of variable thickness and large surface areas, opens up new areas of possible technological applications for these materials.[25] On the other hand, the synthesis of these lanthanide-based polymer electrolytes is in accordance with the new trends in the field of luminescent materials where ligands protecting organic cage-type hosts kinetically inerts, e.g., macrocyclic ligands such as, for instance, cyclams, crown ethers, and cryptands, are used as efficient lanthanide coordinated sites.[26,27] The main prospect of this strategy involves the synthesis of stable supramolecular structures with high luminescence efficiencies employing the so-called *antenna effect*, e.g., absorption of ultraviolet light by the ligand cage-type hosts, an efficient intermolecular energy transfer to the luminescent center and a subsequent high efficient emission.[27]

In the quest for the development of technological applications using POE-based cage-type Eu^{3+} electrolytes two very severe drawbacks were immediately recognized. The electrolytes present a strong tendency to crystallize, which reduces optical quality, and show a high hygroscopic character, which enhances the quenching of Eu^{3+} emission by deactivations via O-H oscillators and makes compulsory handling in an inert atmosphere. In order to suppress problems related to crystallization of the electrolytes a large variety of polymer host structures have been investigated, including polymers with comb-branched backbones, cross-linked networks, block polymers, etc.[1–3] Two other methods employed for decreasing the crystalline nature of POE-based electrolytes (and, consequently, improving their ionic transport properties) are the incorporation in the polymer matrix of small amounts of plasticizers[1–3] and the use of large plasticizing anions as, for instance, (bis)trifluoromethanesulfonate imide (TFSI).[28] In this case, the hygroscopic character of the materials is also reduced due to the bulkiness, flexibility, and charge delocalization of the anion. For lanthanide-based polymer electrolytes the luminescence features of the $EuTFSI_3$ salt incorporated in poly(propylene glycol), PPG, and in low-molecular-weight POE oligomers have been recently reported.[24]

A different route in order to overcome both the crystallization character and the high hygroscopic tendency of lanthanide-based POE electrolytes can be achieved by the sol-gel synthesis of similar luminescent polymers based on organic/inorganic hybrid materials.[29–33]

In recent years the use of the sol-gel approach for the synthesis of a wide range of novel materials has attracted considerable scientific interest.[34] In particular, the advantages of the rich chemistry of silicon-based networks have been employed to synthesize amorphous and transparent hybrid organic/inorganic structures incorporating lanthanide salts.[35–38] The hybrid nature of these matrices improves the lanthanide cation emission and the mechanical stability of the sample, comparing to the conventional silica gel hosts.[35–38] Furthermore, due to the presence of a siliceous backbone skeleton some of the organic/inorganic gels themselves are luminescent between 14 K and room temperature.[38–43] In spite of the potential technological relevance of that emission in several optics and electro-optics devices, such as, for instance, hybrid layers for optical data storage, optical waveguides, stable nonlinear optical materials, sensors or gel glasses dispersed liquid crystals, electrochromics hybrids for smart windows,[35,39] only a limited number of works has been focused on these light-emission features.[38–43]

The relevance of the sol-gel method for the synthesis of a different family of europium-based hybrid materials, classed as ureasils, based on a siliceous backbone to which oxyethylene units are covalently grafted by means of urea linkages was recently shown by our two groups.[29–32] These organically modified silicates are obtained as transparent elastomeric and essentially amorphous thin monoliths—thermally stable up to about 200 °C—and, besides the observed decrease in its crystalline nature and hygroscopic propensity, they clearly present several marked emissions advantages relatively to the analogous Eu^{3+}-based polymer electrolytes. In fact, the ureasil hybrids are room-temperature white light phosphors (multiwavelength emitters) combining narrow yellow-red Eu^{3+} luminescence with broad green-blue emission.[29–32] The white light phosphor nature of these urea cross-linked organically modified silicates has already been reported for the undoped ureasil host, i.e., on the absence of any activator metal ion.[29,30,42,43]

The achievement of full color displays is one of the main challenging tasks on the field of luminescent materials. An interesting class of stable and efficient white photoluminescent silicate materials prepared from an alkoxysilane (similar to the precursor used in the synthesis of the ureasils) and a variety of organic carboxylic acids through a sol-gel route has been recently reported.[40] When heated above ≈ 400 °C, besides a short-lived luminescence ($\leqslant 10$ ns), these hybrids display a bright phosphorescence with a lifetime of several seconds at room temperature.[40] We must also emphasize the set of white light emission complexes based on light emitting diodes (LED's) involving blends of conjugated polymers,[44] multilayer organic dye LED's,[45] and the III-nitride technology associated with conjugated polymers.[46] In the latter systems, as, for instance, the case of InGaN/conjugated polymer hybrid LED's,[46] the blue-light from the InGaN pump is totally (or partially) absorbed and re-emitted as light of a different color by using thicker polymer films. The ability to control the color with the InGaN/conjugated polymer hybrid LED's is achieved by varying the thickness of the conjugated

polymer film and by a prudent choice of the polymer materials.[46]

The present paper gives a detailed description of the luminescence features of white light Eu^{3+}-based hybrids and attempts to determine the local coordination of a lanthanide ion in organic/inorganic xerogels combining the cation luminescence characteristics with its extended x-ray-absorption fine-structure (EXAFS) features. For polymer electrolytes and organic/inorganic hybrids incorporating lanthanide cations this analysis, to the best of our knowledge, has not been done yet. Even for other classes of materials modified by europium salts a limited number of reports have been done up to now dealing with EXAFS studies and with the analysis of the local cation coordination combining EXAFS and luminescence properties.[47,48]

The remainder of the article is organized into four additional sections. In Sec. II we describe the ureasils synthesis and the experimental procedures associated both with the EXAFS and luminescence measurements. The analysis of the EXAFS data for determining the coordination number and the average Eu^{3+} first oxygen neighbors distance, as well as the luminescence spectra (excitation and emission modes) of the Eu^{3+}-based hybrids are presented in Sec. III. In particular, we illustrate an interesting approach to obtaining room-temperature white light emitters by using the Eu^{3+}-based ureasils hybrids in which the ability to tune the emission to colors across the (Commission Internationale de L'Eclairae) (CIE) (1931) chromaticity diagram is achieved either by changing the amount of europium salt incorporated in the ureasil host or the excitation wavelength. In Sec. IV we show that the local environment of Eu^{3+} consists of a continuous distribution of closely similar low-symmetry network sites in which the Eu^{3+} cations are coordinated by the carbonyl groups of the urea moieties, water molecules and, for $U(2000)_n Eu(CF_3SO_3)_3$, by the oxygen ligands of the triflate anions. For the xerogel in which there are four available carbonyl oxygens for each incorporated Eu^{3+}, $U(2000)_{80}Eu(CF_3SO_3)_3$, a possible local charge distribution around the cations is suggested. Furthermore, we demonstrate that the covalency nature of the first coordination shell of the hybrids reported here is low, comparing with analogous POE electrolytes modified by $EuBr_3$, and based on the energy levels assignment, we evaluate a mean radius for the Eu^{3+} nearest ligands distribution. Finally, the concluding remarks are presented in Sec. V.

II. EXPERIMENT

A. Materials

The synthesis of the Eu^{3+}-based xerogels discussed in this work has been described in detail elsewhere.[29,30,49] The sol-gel hybrids contain short highly solvating (OCH_2CH_2) units (≈ 40.5) covalently grafted onto a siliceous network by means of urea bridges and have been designated as ureasils (ureasilicates).[50] The oxyethylene segment is present in doubly functional amines—chemically a,ω-diamine-poly(oxyethylene-co-oxypropylene). The bond between the alkoxysilane precursor and the polyether chains is formed by the reaction of the terminal amino groups of the diamine with the isocyanate group of the precursor used (3-isocyanatepropyltriethoxysilane, Fluka) which leads to the formation of urea bonds (ureapropyltriethoxysilane, UPTES, precursor). The diamine used in this study is commercially designated as Jeffamine ED-2001 (Fluka). The Eu^{3+}-doped ureasils, obtained by the addition of $Eu(CF_3SO_3)_3$ (Aldrich) and $EuBr_3$ (Alpha) to the urea crosslinked hybrid, have been identified by $U(2000)_n EuX_3$, $X = CF_3SO_3$ and Br, where U originates from the word ''urea,'' 2000 indirectly indicates the length of the oligopolyoxyethylene chains and $n = O/Eu$ represents the number of (OCH_2CH_2) monomer units per Eu^{3+} cation. For the $U(2000)_n Eu(CF_3SO_3)_3$ ureasils n varies between 200 and 20, whereas for the $U(2000)_n EuBr_3$ hybrids the salt concentrations investigated are $n = 80$, 40, and 30.

B. Measurements

X-ray-absorption experiments were conducted on the EXAFS station at the LNLS (National Synchrotron Light Laboratory-Brazil) ring operating at 1.37 GeV and 100 mA of nominal current with the beam monochromatized by a Si(111) double-crystal. Spectra were recorded at the Eu L_{III} edge (6977 eV) in the transmission mode with air filled ionization chambers in the detection. Bulk samples were used with thickness adjusted in order to obtain a reasonable absorption coefficient. In the approximation of simple scattering and plane waves, the EXAFS results can be interpreted with the following equation:

$$\chi(k) = \sum_j \frac{N_j}{kR_j^2} F_j(k,\pi) \exp(-2\sigma_j^2 k^2) \times \exp\left(-\frac{2R_j}{\lambda}\right) \sin[2kR_j + \phi_j(k)], \quad (1)$$

where k is the wavevector of the photoelectrons, $F_j(k,\pi)$ is the amplitude of the backscattering of each of the N_j neighboring equivalent atoms localized at a mean bond distance R_j of the absorber atom, σ_j is the Debye-Waller factor, $\lambda(k)$ is the mean free path of the photoelectrons, and $\phi_j(k)$ is the phase shift including the absorber atom (in this case Eu^{3+}) and the backscattering atoms (in this case oxygens).

The EXAFS oscillations $\chi(k)$ have been analyzed by conventional methods including normalization, background removal and Fourier transform of the EXAFS spectra. To determine the structural parameters R, N, and σ_j the Fourier transform method was used.[51] The data were analyzed using the available simulations programs on Macintosh computer.[52] To obtain Fourier transforms, EXAFS spectra were multiplied by the factor k^2 and a Kaiser apodization window was used between 3 and 10 $Å^{-1}$, with $\tau = 2.5$. Polycrystalline Eu_2O_3 powder was used as reference during simulations for the first coordination sphere around the europium atom (six oxygen atoms at a mean distance of 2.371 Å).

Luminescence spectra were recorded in the temperature range of 14–300 K with a resolution of 0.05 nm. The luminescence was excited by a 1000 W xenon arc lamp (Kratos LH151N/1S) and recorded using a 0.25-m monochromator (Kratos GM-252)—fitted with a 1180-grooves/mm grating—and a 1-m Czerny-Turner spectrometer (1704 Spex)—fitted with a 1200-grooves/mm grating—coupled to a photomultiplier (Hamamatsu R928). All the spectra were corrected for

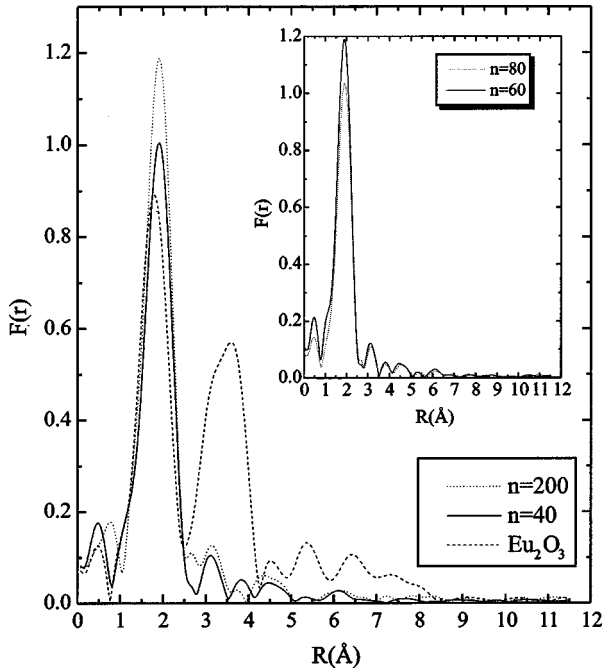

FIG. 1. Radial structural functions around Eu^{3+} for standard Eu_2O_3 (dashed line) and for $U(2000)_nEu(CF_3SO_3)_3$, $n=200$ (dot line) and $n=40$ (full line). Inset shows the radial structural functions for $U(2000)_{80}Eu(CF_3SO_3)_3$ (dotted line) and $U(2000)_{60}Eu(CF_3SO_3)_3$ (solid line).

the detector response. The experimental setup used has been described in detail previously.[18]

III. RESULTS

A. Extended x-ray-absorption fine structure

After carrying out routine procedures for data normalization and extraction of the EXAFS signal from experimental absorption spectra the pseudoradial distribution functions were obtained by Fourier analysis. Figure 1 shows the modulus of the Fourier transforms thus obtained for the hybrids and also for the standard Eu_2O_3. The main observation concerns the presence of only one strong peak in the Fourier transforms of the hybrids, meaning that order exists for these systems only for the first Eu^{3+} ions neighbors range.

In order to obtain quantitative results and to interpret the amplitude variations observed in the first peak of the Fourier transforms a simulation of the EXAFS spectra was performed. The first coordination sphere of Eu^{3+} was characterized by fitting filtered EXAFS spectra with Eq. (1), using phase and amplitude functions obtained from the standard Eu_2O_3 spectrum. Figure 2 shows experimental and calculated spectra. Good fits were obtained for all samples. The EXAFS results are summarized in Table I. These results suggest a decrease in the coordination number with the increase in the relative Eu^{3+} concentration between $n=200$ and $n=40$. Furthermore, the decrease of the Debye-Waller disorder factor

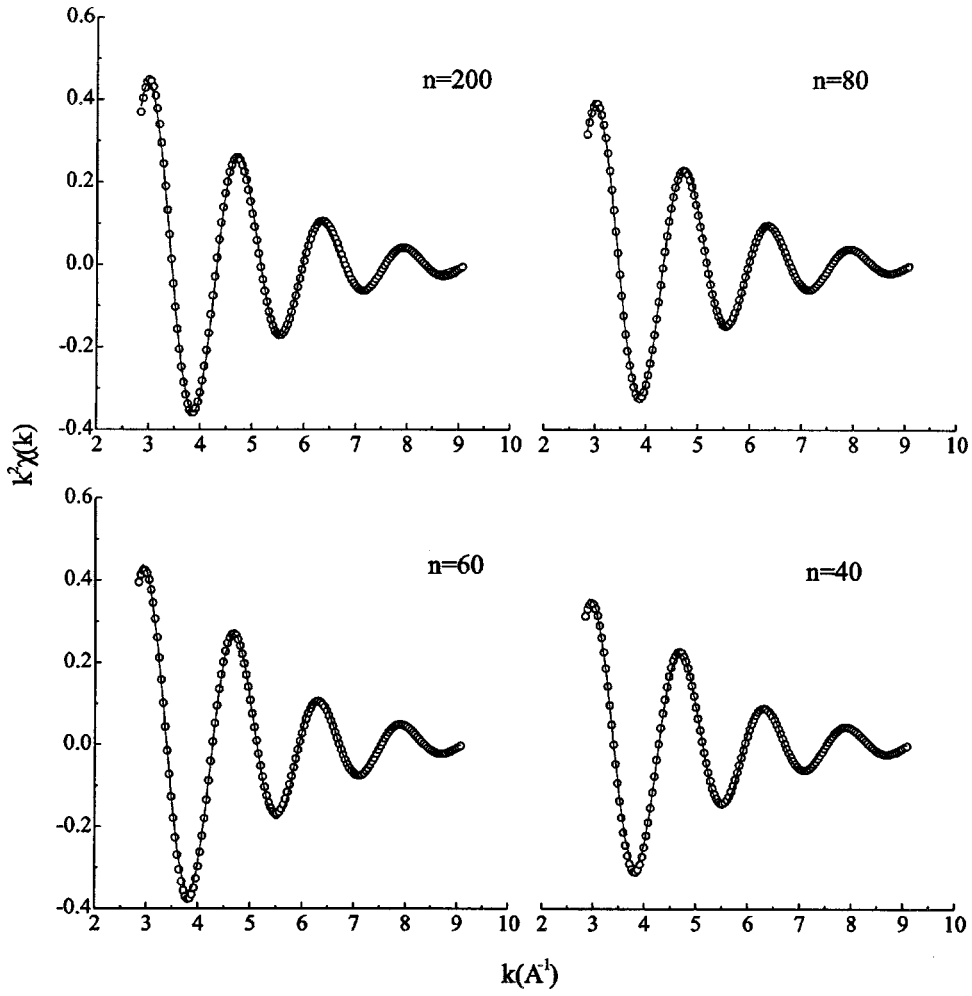

FIG. 2. k^2-weighted Fourier-filtered EXAFS of the Eu^{3+} first coordination shell (circles) and best fit (solid line) for $U(2000)_nEu(CF_3SO_3)_3$, $n=200$, 80, 60, and 40.

TABLE I. Room-temperature EXAFS simulation at the Eu L_{III} edge. N is the first-neighbors number, R (Å) the Eu-O mean distance and $\Delta\sigma$ (Å^2) the Debye-Waller factor.

	$N(\pm 1)$	$R(\pm 0.05)$	$\Delta\sigma^2(\pm 0.0005)$
$U(2000)_{200}Eu(CF_3SO_3)_3$	12.8	2.48	0.0072
$U(2000)_{80}Eu(CF_3SO_3)_3$	11.2	2.48	0.0068
$U(2000)_{60}Eu(CF_3SO_3)_3$	11.8	2.48	0.0055
$U(2000)_{40}Eu(CF_3SO_3)_3$	9.7	2.49	0.0050

in this salt concentration range indicates the tendency of the dispersion of the Eu-O distances to decrease.

B. Photoluminescence spectra

Figure 3 shows the excitation spectrum for $U(2000)_{20}Eu(CF_3SO_3)_3$ ($\lambda_{emiss.}=617$ nm) at 14 K. The sharp lines were assigned to intra-$4f^6$ transitions between the $^7F_0$ and the $^5D_{1-3}$, $^5L_6$ levels, whereas the broad band is ascribed to intraconfigurational ligands-to-Eu^{3+} charge-transfer transitions (CTT). This band lies in the same energy region of the $^7F_0\rightarrow{}^5L_6$ and $^7F_0\rightarrow{}^5D_3$ transitions. As temperature rises from 14–300 K, the line intensity is generally reduced by $\approx 40\%$.

With the increase of the $Eu(CF_3SO_3)_3$ content from $n=200$ to $n=20$ we notice drastic changes on the CTT maximum position. While for $200\geqslant n\geqslant 80$ and for $40\geqslant n\geqslant 20$ the CTT maximum shifts towards the low-energy region of the spectrum, for salt concentration between $n=80$ and $n=40$ the opposite trend is observed, that is, the CTT maximum shifts towards the high-energy region of the spectrum (inset of Fig. 3).

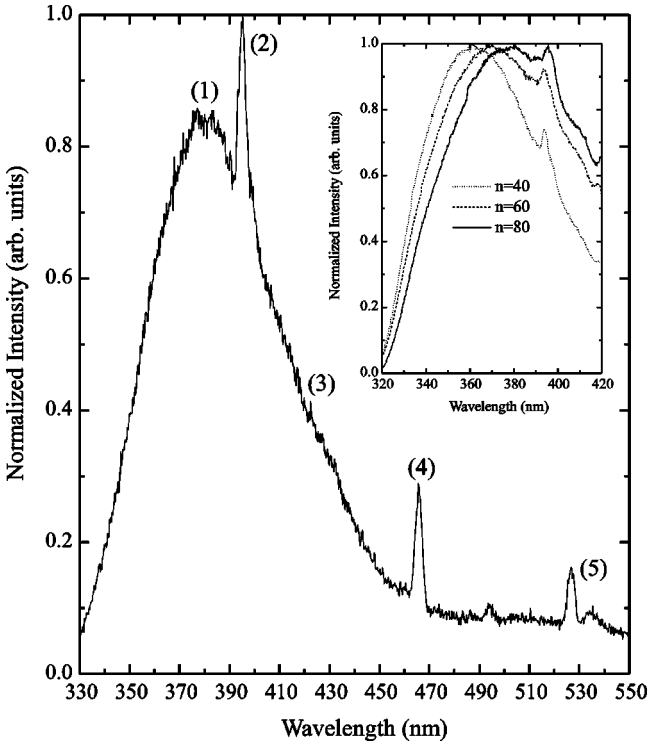

FIG. 3. Excitation spectrum ($\lambda_{emiss.}=617$ nm) for $U(2000)_{20}Eu(CF_3SO_3)_3$ at 14 K. Inset shows the CTT wavelength region for $U(2000)_nEu(CF_3SO_3)_3$, $n=80$, 60, and 40. (1): CTT; (2), (3), (4): $^7F_0\rightarrow{}^5L_6$, $^5D_3$, $^5D_2$; (5): $^7F_0\rightarrow{}^5D_1$.

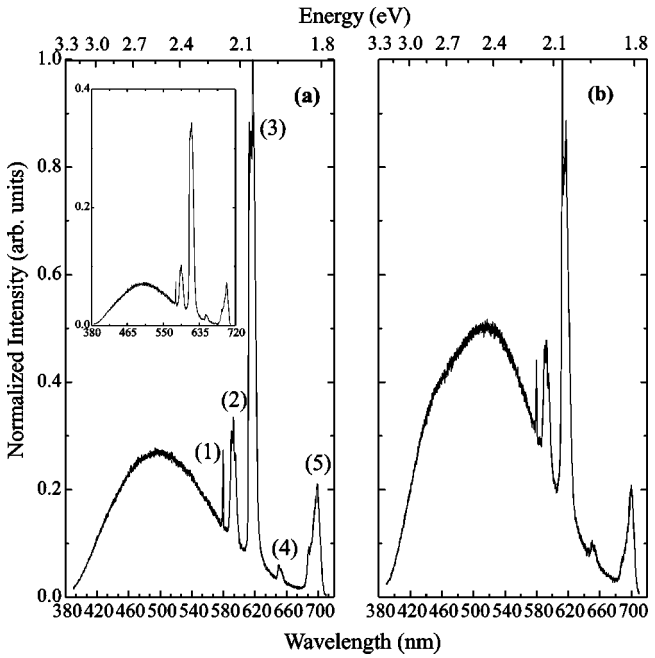

FIG. 4. Emission spectra ($\lambda_{exc.}=375$ nm) for $U(2000)_{90}Eu(CF_3SO_3)_3$ (a) and $U(2000)_{80}EuBr_3$ (b) at 14 K. (1), (2), (3), (4), (5): $^5D_0\rightarrow{}^7F_{0,1,2,3,4}$. Inset shows the reduction of the integrated intensity observed in $U(2000)_{85}Eu(CF_3SO_3)_3$ ($\lambda_{exc.}=375$ nm) when the temperature rises from 14–300 K.

It is known that a shift of the charge-transfer transition frequencies toward the high-energy region of the spectrum is related to an increase of the effective charge of the lanthanide cation,[53] and thus to a decrease of the tendency of the first ligands to bond covalently to the metal ion (see, for instance, Ref. 54). This behavior may be induced by an increase on the cation first ligands distances and/or by a reduction in the number and in the effective charge of the neighbor ligands. The EXAFS results (Table I) suggest that the reduction in the number of oxygen ligands between $n=80$ and $n=40$ may account for the mentioned increase on the effective valence of the europium ions and therefore for the corresponding decrease on the covalency nature of the Eu^{3+} first coordination shell.

Figure 4 shows the 14 K emission spectra ($\lambda_{exc.}=375$ nm) for the xerogels $U(2000)_{90}Eu(CF_3SO_3)_3$ and $U(2000)_{80}EuBr_3$ recorded at the excitation wavelength for which the europium integrated relative intensities are stronger. The narrow lines were assigned to transitions between the first excited state, $^5D_0$, and the $^7F_{0-4}$ levels of the ground multiplet. Luminescence from higher excited states such $^5D_1$ is not detected indicating very efficient nonradiative relaxation to the $^5D_0$ level. The observed intra-$4f^6$ transitions are mainly of electric dipole (ED) nature except the $^5D_0\rightarrow{}^7F_1$ lines which have a predominant magnetic dipole (MD) character. As temperature rises from 14–300 K the line intensity is generally reduced by $\approx 50-60\%$, inset of Fig. 4(a).

The broad green-blue band seen in Fig. 4, already observed in the luminescence spectra of the undoped

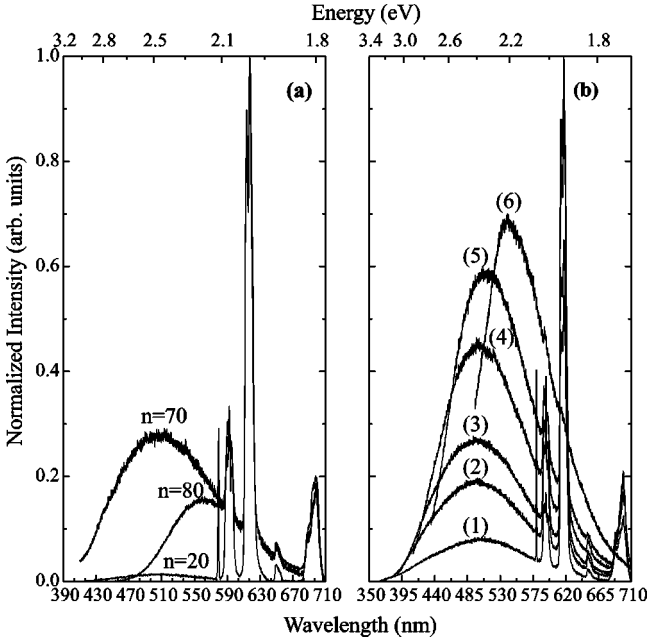

FIG. 5. (a) Emission spectra for $U(2000)_n Eu(CF_3SO_3)_3$, $n=80$ ($\lambda_{exc.}=375$ nm), 70 ($\lambda_{exc.}=395$ nm), and 20 ($\lambda_{exc.}=365$ nm) at 14 K. (b) Emission spectra for $U(2000)_{90}Eu(CF_3SO_3)_3$ at 14 K recorded for several excitation wavelengths: (1), (2), (3), (4), (5), (6): 350, 365, 375, 420, 468, and 482 nm.

ureasil,[29,30,32,42,43] may be ascribed to electron-hole radiative recombinations occurring in the inorganic siliceous backbone. In fact, as is the case of other silicon-based materials mentioned in the literature,[55–57] electron-hole recombinations involving strongly correlated electron-hole exciton states or radiative tunneling between localized states of the electrons and holes may be the mechanisms which account for the observed broad band emission. However, attending to the long lifetimes reported for that emission, $\approx 10^{-2}$ s,[42] we cannot discarded an eventual contribution from the N-H groups of the urea cross linkages, as the emission spectra of the diamine and the UPTES precursors show.

The relative intensity and the energy range of the broad green-blue emission strongly depend on the amount of triflate salt incorporated in the hybrid matrix, as the 14 K emission spectra for $U(2000)_{80}Eu(CF_3SO_3)_3$ ($\lambda_{exc.}=375$ nm), $U(2000)_{70}Eu(CF_3SO_3)_3$ ($\lambda_{exc.}=395$ nm), and $U(2000)_{20}Eu(CF_3SO_3)_3$ ($\lambda_{exc.}=365$ nm) show, Fig. 5(a). These excitation wavelengths correspond to the values for which the europium integrated relative intensities are stronger. In addition, as the excitation wavelength increases from 350–468 nm, the intensity of the broad emission increases, relatively to the Eu^{3+} lines, and there is a shift towards the low-energy regions of the spectrum, Fig. 5(b), also already reported for the undoped ureasil hybrid.[42,43]

A set of real time frames showing the ureasil white light emission is displayed in Fig. 6 for $U(2000)_{80}EU(CF_3SO_3)_3$ at 14 K. These pictures were extracted from a split video film recorded during 1 s after the laser beam (Ar ion) was turned off. The long-lived luminescence of any other phosphors can be thus visualized in real time by using the same procedure. The ureasil white light emission is achieved by a mechanism which is completely different than the one characteristic of multiwavelength com-

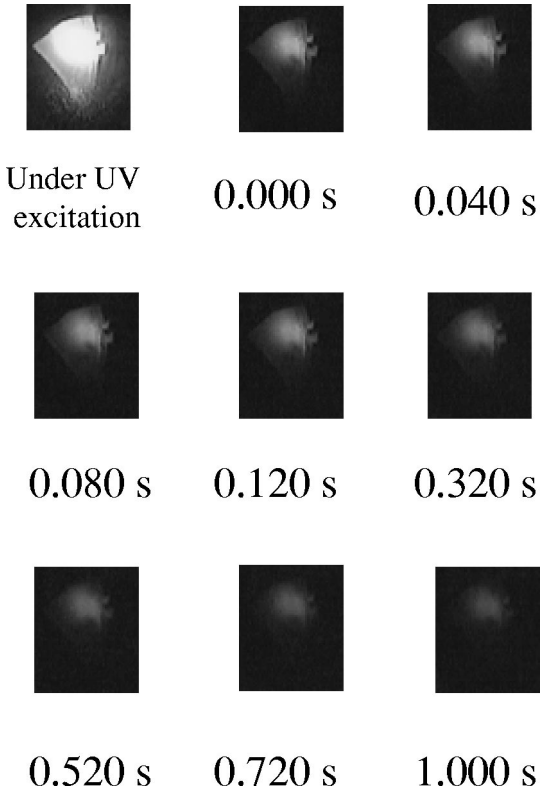

FIG. 6. A set of real-time frames illustrating the white light emission of $U(2000)_{80}Eu(CF_3SO_3)_3$ at 14 K under UV excitation (331.1 and 351.4 nm) and during 1 s after the laser beam (100 mW) was turned off.

plexes based on light emitting diodes.[44–46] As nondetectable absorption of the broad green-blue component by the Eu^{3+} luminescent centers is observed, the ureasils luminescence spectra superpose that broad green-blue band to a series of yellow-red narrow Eu^{3+} lines and to the eye the hybrids appeared to be white, even at room temperature. This absence of self-absorption by the lanthanide cation is, as it is mentioned for InGaN/conjugated polymer hybrid LED's,[46] a critical advantage. On the other hand, the ability to tune the ureasils emission to colors across the (CIE) (1931) chromaticity diagram is readily achieved either by changing the amount of europium salt incorporated in the ureasil host or the excitation wavelength, Figs. 5(a) and (b). Moreover, any sign of luminescence degradation is detected (both in the undoped and doped hybrids) under a prolonged irradiation by the photoexcitation conditions used. All these features, in turn, stress the remarkable potential of this interesting class of multiwavelength hybrid phosphors.

When compared with the emission spectra of the undoped ureasils,[29,30,42,43] the green-blue emission band is shifted towards lower energies. The deconvolution of the undoped hybrid light emission displays, for excitation wavelengths between 350 and 400 nm (3.10–3.54 eV), two unshaped Gaussian bands, in the blue (≈ 2.6 eV) and in the purplish-blue (≈ 2.8–2.9 eV) regions.[42,43] Due to a different time dependence, these two bands are distinctly observed by time-resolved spectroscopy.[42] In the case of the doped hybrids with concentrations $90 \geqslant n \geqslant 20$, the deconvolution curve-fitting procedure of the broad emission reveals, for excitation wavelengths between 350 and 420 nm (2.95 and 3.54 eV),

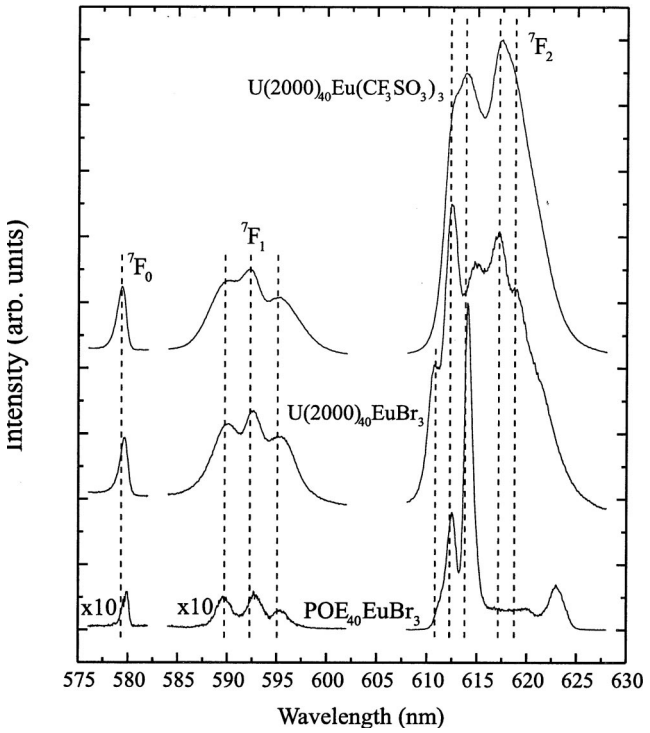

FIG. 7. The local-field splitting of the $^5D_0 \rightarrow {}^7F_{0-2}$ transitions in $U(2000)_{40}Eu(CF_3SO_3)_3$, $U(2000)_{40}EuBr_3$, and $POE_{40}EuBr_3$.

also the presence of two bands, in the green and in the blue/purplish-blue spectral regions. However, for excitation wavelengths between 468 and 482 nm (2.65 and 2.57 eV), the luminescence spectra were fitted just to the green component, with the exception of $U(2000)_{80}Eu(CF_3SO_3)_3$ in which the two bands are distinctly present. The curve-fitting procedure adopted is exactly the same that have been reported elsewhere for the undoped ureasils.[42,43] For that concentration range ($90 \geqslant n \geqslant 20$) and for excitation wavelengths between 350 and 482 nm the energy of the green component is fitted around 2.2–2.5 eV, 2.0 eV for $n=80$, whereas the values found for the blue/purplish-blue band are approximately equal to 2.5–2.9 eV, 2.3 eV for $n=80$. Comparing with the spectra of the undoped ureasil the energy of these two bands is redshifted by $\approx 0.1-0.3$ eV for all the ureasils samples investigated here, except for $n=80$ where this difference is $\approx 0.5-0.7$ eV.

In the next section, we will relate the emission features and the EXAFS data discussed above to the local coordination of Eu^{3+} in the ureasil hybrids.

IV. LOCAL COORDINATION OF Eu^{3+}

The number of Stark components identified for the $^7F_{0,1,2}$ levels in $U(2000)_nEu(CF_3SO_3)_3$ hybrids is 1, 3, and 4, respectively (Fig. 4). While in the $^7F_1$ manifold the three Stark levels are well defined, there is some uncertainly in the identification and energy assignment of the lower-energy split component of the $^7F_2$ level. The weak intensity of the $^5D_0 \rightarrow {}^7F_3$ does not allow an accurate energy assignment of the $^7F_3$ Stark components and for the $^7F_4$ state at least five split components are distinctly detected. As Figs. 5(a) and (b) show, these number of Stark levels does not vary either with the excitation wavelength or cation concentration.

Figure 7 compares the J-degeneracy splitting of the $^7F_{0,1,2}$ levels in $U(2000)_{40}Eu(CF_3SO_3)_3$, $U(2000)_{40}EuBr_3$, and $POE_{40}EuBr_3$. The relative intensity of the $^5D_0 \rightarrow {}^7F_{0,1}$ transitions is approximately an order of magnitude smaller for the Eu^{3+}-based POE electrolyte. When the $^5D_0 \rightarrow {}^7F_0$ transition is allowed by the local symmetry group, its intensity can be, in general, explained by J-mixing effects involving the mixing of the $^7F_0$ and $^7F_2$ levels, through the effective ligand-field Hamiltonian.[58] The increase observed in the ratio between the $^5D_0 \rightarrow {}^7F_0$ and the $^5D_0 \rightarrow {}^7F_2$ transitions, from 0.004–0.009 in POE-based electrolytes to 0.018–0.033 in the ureasils, indicates that the J-mixing effects are much more relevant in the latter host.

In what concerns the splitting of the $^7F_2$ level, while in the $U(2000)_{40}EuBr_3$ and $POE_{40}EuBr_3$ samples five different Stark components are identified (full J-splitting degeneracy), in the $U(2000)_{40}Eu(CF_3SO_3)_3$ ureasil only four components could be detected. The higher-energy split level observed in the $EuBr_3$-based films at about 613 nm is not observed in any of the different concentrations of $U(2000)_nEu(CF_3SO_3)_3$ studied.

The presence of the $^5D_0 \rightarrow {}^7F_{0,3}$ transitions, the J-degeneracy splitting and the observation of the same number of local-field split components over the entire range of excitation wavelength used, indicate only one low-symmetry environment for the Eu^{3+} cations in the hybrid materials reported here. However, we should stress that the calculated values of the $^5D_0 \rightarrow {}^7F_0$ full width at half maximum intensity, between 19 and 31 cm^{-1}, point out that the Eu^{3+} cations are accommodated in a continuous distribution of closely similar network sites. This distribution is normally observed for Eu^{3+}-based oxide glasses and has been also reported for other polymer-based materials modified by europium salts.[17,22]

The previously reported local coordination of Eu^{3+} in POE and POP electrolytes is approximately a C_{2v} site symmetry.[15,18,19] This same local geometry has also been proposed for $EuCl_3$ incorporated in POE oligomers.[22] However, for the $U(2000)_nEu(CF_3SO_3)_3$ hybrids the J-splitting degeneracy of the $^7F_2$ level and the overall broad envelope of the $^5D_0 \rightarrow {}^7F_2$ transition strongly suggest that the Eu^{3+} site symmetry must be of higher order than C_{2v}. The coordination established between the cations and the oxygens of the triflate anions, recently discussed in a Fourier transform infrared (FTIR) study,[59] may account for the increase of the local site symmetry of the $U(2000)_nEu(CF_3SO_3)_3$ hybrids, when compared to $U(2000)_nEuBr_3$ and POE_nEuBr_3. In the range of n investigated for both $U(2000)_nEu(CF_3SO_3)_3$ and $U(2000)_nEuBr_3$ hybrids, the FTIR results clearly indicate that the europium ions are coordinated by the carbonyl oxygens of the urea moieties and no spectral evidences have been found for the coordination by the ether oxygens of the polyether chains,[59] unlike the situation observed in Eu^{3+}-based POE and POP electrolytes.

Accordingly to the cation coordination to the urea bridges is convenient to express the salt concentration also in terms of the number of available carbonyl oxygens per incorporated Eu^{3+} cation. Representing the salt concentration by this number of accessible carbonyl oxygens the hybrid structure of $n=80$ corresponds to a particular situation in which there

are four available carbonyl oxygens for each incorporated europium ion. For salt concentration greater than $n=20$, for which the ratio between the number of carbonyl oxygens and the incorporated Eu^{3+} is 1:1, all the urea bridges are coordinated to one cation and, consequently, there are some Eu^{3+} ions which are coordinated to the ether oxygens of the polymer chains (as the FTIR analysis shows, Ref. 59).

Taking into account the coordination number in the $U(2000)_n Eu(CF_3SO_3)_3$ hybrids determined by EXAFS (Table I), the infrared results mentioned above and at last the photoluminescence indication that the cation site symmetry group in these hybrids must be of higher order than C_{2v}, we are able to suggest a possible local charge distribution around Eu^{3+} for the case of the $U(2000)_{80}Eu(CF_3SO_3)_3$ xerogel. For this salt concentration the FTIR results regarding the triflate spectral region indicate that one of the three available triflate ion is ''free'' (that is, this ion do not participate in ion pairing or aggregate formation).[30,32,59] Moreover, the oxygens atoms of the remaining two SO_3 end groups are bonded in two different fashions.[59] One is unequivocally in a tridentate coordination, whereas the other is involved in a mono- or bidentate coordination.[59] Thus as for this salt concentration the coordination number is around 11 (Table I) and there are four available carbonyl oxygens for each incorporated europium ion, the Eu^{3+} first coordination shell can be formed by those four carbonyl oxygens, by five oxygens from the SO_3 end groups of the triflate anion (four if we consider the monodentate configuration) and by two (or three) water molecules.

We will test next this hypothesis for the local structure of the $U(2000)_{80}Eu(CF_3SO_3)_3$ xerogel by expressing its $^5D_0 \rightarrow {}^7F_0$ observed energy in terms of a recent description related to the so-called *nephelauxetic effect*.[60]

A. Covalency of the Eu^{3+} first coordination shell

The energy of $^5D_0 \rightarrow {}^7F_0$ is usually related to the nephelauxetic effect, which has been ascribed by Jørgensen[16,61,62] to the influence of covalency contributions of the first ligands shell to the reduction of the Eu^{3+} attractive potential, provoking a diminution of the interelectronic electrostatic and spin-orbit parameters, relative to their free ion values.

Recently the redshift observed in the $^5D_0 \rightarrow {}^7F_0$ energy for a series of Eu^{3+} complexes, with respect to the value calculated for gaseous Eu^{3+} ($17\,374\,cm^{-1}$),[63] was related with the nephelauxetic effect by means of a phenomenological equation:

$$\Delta E \equiv E(^5D_0 \rightarrow {}^7F_0)_{\text{complex}} - E(^5D_0 \rightarrow {}^7F_0)_{\text{gaseous}} = C_N[n_1 \cdot \delta_1 + n_2 \cdot \delta_2 + \cdots + n_j \cdot \delta_j] \quad (2)$$

in which C_N is the total number of Eu^{3+} first ligands, n_j is the number of atoms of type j in the first coordination shell, and δ_j is an adjusted parameter, which measures the tendency of a particular atom to bond covalently with the Eu^{3+} cation.[60] The results obtained using Eq. (2) show that the ability to produce a nephelauxetic effect in Eu^{3+} complexes, and consequently to reduce its $^5D_0 \rightarrow {}^7F_0$ energy and the covalency of the bonds which form the Eu^{3+} first coordination shell, depends on the ligand coordination number and on the particular characteristics of their chemical environments. Despite its phenomenological nature, the main results of this model nicely agree with a series of *a priori* arguments related with the role on covalency and local polarization induced by different local environments. In particular, it is realistic to consider, as the model points out, that the Eu^{3+} coordination to different types of oxygen-based environments (such as, for instance, oxygens of water molecules or ether oxygen ligands), as well as changes on the total coordination number may cause different degrees of covalency and local polarization in the lanthanide first coordination shell.

Considering the Eu^{3+} environment proposed above for $U(2000)_{80}Eu(CF_3SO_3)_3$, that is an 11-fold coordination involving four carbonyl oxygens, five (or four) oxygen atoms from the triflate anions—coexistence of tri- and bidentate (monodentate) coordinations for the two coordinated SO_3 end groups), and two (or three) water molecules,—the predicted $^5D_0 \rightarrow {}^7F_0$ energy shift derived from Eq. (2), $-122.0\ cm^{-1}$ (or $-120.6\ cm^{-1}$ in the monodentate case), agrees well with the experimental value, $-122.2\,cm^{-1}$. This calculation was performed using the δ_j presented in Table 2 of Ref. 60 for carbonyl and nitrate oxygens, as the δ_j value for the SO_3 group is unknown. We should stress that despite the tendency of the SO_3 group to bond covalently with the Eu^{3+} cation is considered similar to the one associated with the NO_3 oxygens, the difference between the predicted and calculated values is within the correlation uncertainty reported for the δ_j and C_N coefficients, $\pm 3\ cm^{-1}$.[60]

In this context, we note that the predicted $^5D_0 \rightarrow {}^7F_0$ energy shift derived from Eq. (2) for $POE_{12}EuBr_3$, in which the coordination number was estimated based on two independent methods as 10–11 ether oxygens,[23] agrees, also, very well with the experimental values. The observed result is $-105.8\,cm^{-1}$ and the predicted one is $-105.6\,cm^{-1}$, for ten nearest ligands.

The ratio between the integrated intensity of the $^5D_0 \rightarrow {}^7F_2$ and the $^5D_0 \rightarrow {}^7F_1$ transitions, I_{0-2}/I_{0-1}, is used in lanthanide-based systems as a probe of changes on the nature of the cation local surroundings.[54,58,61,62,64] For the $U(2000)_n Eu(CF_3SO_3)_3$, the values obtained for I_{0-2}/I_{0-1} ranging from 5.37, $n=80$, to 2.88, $n=30$. For the three analogous $U(2000)_n EuBr_3$ xerogels I_{0-2}/I_{0-1} is found to be 3.63 ($n=80$), 4.22 ($n=40$), and 2.95 ($n=30$). With the exception of the $n=80$ salt concentration, for which the europium triflate-based ureasil I_{0-2}/I_{0-1} ratio is approximately 1.5 times greater than the one calculated for $U(2000)$-$EuBr_3$, the hypersensitive ratio values are similar for the two series of hybrids. However, comparing these values with the ones found for the $POE_n EuBr_3$ and $POP_n EuBr_3$ electrolytes[15,18,19] we noted that they are consistently greater (at least by a factor of 2) for the latter materials, in accordance with the lower relative intensity of the $^5D_0 \rightarrow {}^7F_1$ transition in POE-based electrolytes, see Fig. 7.

The increase of the I_{0-2}/I_{0-1} ratio was ascribed previously to an increase of the covalency and of the polarization of the local vicinities of the Eu^{3+} cations (short-range effects).[54,58,62] Based on these relations, the observed decrease in the I_{0-2}/I_{0-1} ratio for the ureasil hybrids, when compared to the values found for the Eu^{3+} POE- and POP-based electrolytes, may thus be related to a decrease on the

covalency of the Eu^{3+} first coordination shell in the former materials. The fact that in the ureasil hybrids the europium cations are coordinated by the carbonyl groups of the urea bridges—and, in the case of $U(2000)$-$Eu(CF_3SO_3)_3$ by oxygens of the SO_3 end group of the triflate anions—may induce a rather low covalency in the Eu^{3+} local environments than the ones characteristic of vicinities of POE-POP-based electrolytes, formed by Eu^{3+}-ether oxygens bonds. This suggestion is in agreement with the results obtained above regarding the redshift of the $^5D_0 \rightarrow {}^7F_0$ energy treated in terms of the phenomenological δ_j covalent parameters, Eq. (2). In fact, as we see from Fig. 7, the value obtained for this redshift is lower for the $U(2000)_{40}Eu(CF_3SO_3)_3$ and $U(2000)_{40}EuBr_3$ hybrids, -113.3 and -122.2 cm^{-1}, respectively, than for the $POE_{40}EuBr_3$ electrolyte, -128.2 cm^{-1}. Therefore on the basis of the arguments discussed above the $^5D_0 \rightarrow {}^7F_0$ energy will decrease from its free-ion value with increasing Eu^{3+}-ligand covalency and, thus, the Eu^{3+}-ether oxygens bonds involved in the first coordination shell in $POE_{40}EuBr_3$ have a more effective covalent nature than the Eu^{3+}-carbonyl oxygens and Eu^{3+}-SO_3 bonds associated with the ureasils. This is exactly the conclusion derived from the comparison between the I_{0-2}/I_{0-1} ratios found for the ureasil hybrids and for the Eu^{3+} POE- and POP-based electrolytes.

Another argument which corroborate the assertion of a more effective covalent nature of the Eu^{3+} local environments in POE- and POP-based electrolytes is the energy of the intraconfigurational ligands-to-Eu^{3+} charge-transfer transitions. In these electrolytes the $^7F_0 \rightarrow {}^5L_6$ transition is superposed to the maximum position of the CTT at around 390–395 nm[14,18] and therefore its energy is lower then the maximum value observed in the $U(2000)_nEu(CF_3SO_3)_3$ hybrids ($n=80$, inset of Fig. 3), for which this energy difference is $\approx 500-600\ cm^{-1}$. As we have mentioned in the discussion of the excitation spectra, Sec. III, a decrease of the CTT maximum energy is related to a decrease of the cation effective charge, which corresponds to an increase of the covalency nature of the Eu^{3+} first coordination shell. We notice that the increase of the tendency of the first ligands to bond covalently to the metal ion in POE- and POP-based electrolytes with $100 \geqslant n \geqslant 20$ may be induced by an increase in the number of Eu^{3+} first ligands or in their effective charge. This is entirely compatible with the results found for the coordination number in POE- and POP-based electrolytes which point out a number of first neighbors around 10–11 for $n=12$,[23] whereas in the ureasil hybrids this number is observed for samples with much lower salt concentration, $n \geqslant 60$. On the other hand, the hypothesis of a lower average cation first ligands distance, which, as we have mentioned in Sec. III, may also account for the increase of covalency, is totally discarded as the calculated average radius for the POE- and POP-based electrolytes is approximately the same than the ones reported here (2.4–2.5 Å).[16] Relating the hypersensitive I_{0-2}/I_{0-1} ratio with the local polarization of the Eu^{3+} first coordination shell,[58,62] we may also infer that the Eu^{3+} ion is in a highly polarizable chemical environment in POE- and POP-based electrolytes than in the analogous ureasil hybrids.

Using the same arguments, the maximum I_{0-2}/I_{0-1} value and the CTT minimum energy observed for $n=80$ in the $U(2000)_nEu(CF_3SO_3)_3$ hybrids, may indicate a greater degree of covalency for the Eu^{3+} first coordination shell in this salt concentration. The existence in this salt concentration of four available carbonyl oxygens per each incorporated cation is certainly the main reason which account for the greater tendency of the first ligands to bond covalently to the metal ion.

In the context of this discussion, we must emphasize that the hypersensitive I_{0-2}/I_{0-1} ratio may also be related with the odd parity ligand-field parameters, $B_{k,q}$ (k odd), in such a way that the intensity of the $^5D_0 \rightarrow {}^7F_2$ transition increases with increasing the distortion (on average) of the local-field around the Eu^{3+} cations. Therefore a greater I_{0-2}/I_{0-1} ratio may correspond to a more distorted (or asymmetry) local cation environment.[22,24,54,64] The intensity of the hypersensitive $^5D_0 \rightarrow {}^7F_2$ transition and, consequently, the variation of the I_{0-2}/I_{0-1} ratio depend thus on the balance between the contributions of the odd parity $B_{k,q}$ parameters and of the covalency degree of the Eu^{3+} first ligand oxygens bonds, which induce the admixture of the $4f^5 5d$ states into $4f^6$ levels. However, from the results presented above and attending to some theoretical results obtained in the last years that pointed out the significant amount of mixing between the f electrons and the extended states of the host lattice,[66] we believe that the contribution of the covalency degree of the Eu^{3+} first coordination shell must be dominant to account for the different I_{0-2}/I_{0-1} ratios observed in the ureasils and in the POE- and POP-based electrolytes.

B. A mean radius for the Eu^{3+} first coordination shell

The measured energetic configuration of Eu^{3+} in $U(2000)_nEu(CF_3SO_3)_3$ and $U(2000)_nEuBr_3$ was modeled in terms of a superposition of a free ion Hamiltonian and a local-field perturbation representing the ion's nearest ligands interaction potential. The free ion Hamiltonian (the only term treated in this work) includes the electrostatic, the spin orbit and other less relevant terms, each of which is characterized by a set of phenomenological parameters simulating the barycenters of the observed transitions. Due to the small number of levels observed, only the electrostatic and spin-orbit interactions, phenomenologically expressed by the Slater integrals F^k $(k=2,4,6)$ and the spin-orbit coupling parameter ζ, respectively, were considered here, with $F^{4,6}$ calculated from the hydrogenic ratios F^4/F^2, F^6/F^2. This enabled writing the free ion contribution in terms of only the two parameters F^2 and ζ, which were then determined by adjusting the observed barycenters to the eigenvalues of the $^7F_{0-4}$ free ion Eu^{3+} matrices. Using a microscopic model originally proposed by Morrison[65,67] for the calculation of the observed decrease in the shifts ΔF^k and $\Delta\zeta$ (differences between F^k and ζ in a complex and their corresponding free ion values), Carlos and Videira[16] defined a mean radius specifying an average lanthanide-nearest ligands distance:

$$\overline{R} = \frac{1}{2}\sum_{k=4,6}\left[\frac{(k+1)\rho_k^2}{(\hbar/mc)^2}\left|\frac{\Delta\zeta_{obs}}{\Delta F^k_{obs}}\right|\right]^{1/(2k-2)}$$

$$= \frac{1}{2}\left\{\left[\frac{5\rho_4^2}{(\hbar/mc)^2}\left|\frac{\Delta\zeta_{obs}}{\Delta F^4_{obs}}\right|\right]^{1/6} + \left[\frac{7\rho_6^2}{(\hbar/mc)^2}\left|\frac{\Delta\zeta_{obs}}{\Delta F^6_{obs}}\right|\right]^{1/10}\right\}, \quad (3)$$

where empirically determined values were used for $\Delta F^{4,6}$ and $\Delta\zeta$, and where $\rho_{4,6}$ are corrections to the Hartree-Fock expectation values of the $4f$ electrons radial distances.[67] Here we call attention to the fact that the exponents presented in Eqs. (5) and (6) of Ref. 16, $-2k+2$ and -2, -6, and -10, respectively, should be replaced by the correct ones, $1/(2k-2)$ and $\frac{1}{2}$, $\frac{1}{6}$, and $\frac{1}{10}$.

For the $U(2000)_n Eu(CF_3SO_3)_3$ hybrids, n between 90 and 40, the results obtained, $\overline{R}=2.4$ Å, are quite similar. However, for the high-salt concentration region, $n=20$ and 30, $\overline{R}$ rises to 2.6 Å for $n=30$ and decreases to 2.5 Å for $n=20$. There is a very good agreement (within 5%) between these results and the EXAFS determination of the europium first ligands distances. On the other hand, in the case of $U(2000)_n EuBr_3$, $\overline{R}$ is 2.6 Å for $n=80$ and 30, and 2.4 Å for $n=40$.

V. CONCLUDING REMARKS

We have demonstrated an approach to obtaining room temperature white light emission by using a class of Eu^{3+}-based hybrid xerogels, $U(2000)_n Eu(CF_3SO_3)_3$, $200 \geqslant n \geqslant 20$, and $U(2000)_n EuBr_3$, $n=80$, 40, and 30. The luminescence spectra of these multiwavelength phosphors combine a broad green-blue band (related to radiative recombinations occurring in the ureasil backbone) with sharp yellow-red intra-$4f^6$ $^5D_0 \rightarrow {}^7F_{0-4}$ transitions. Nondetectable absorption of the broad green-blue component by the Eu^{3+} luminescent centers is observed and to the eye all the hybrid films appeared to be white, even at room temperature. Color tunability across the (CIE) (1931) chromaticity diagram was easily obtained changing both the salt concentration and the excitation wavelength.

Extended x-ray-absorption fine-structure measurements were carried out in some of the $U(2000)_n Eu(CF_3SO_3)_3$ xerogels ($n=200$, 80, 60, and 40). The obtained coordination numbers N ranging from 12.8, $n=200$, to 9.7, $n=40$, whereas the average Eu^{3+} first neighbors distance R is 2.48–2.49 Å.

The presence of the $^5D_0 \rightarrow {}^7F_{0,3}$ transitions, the J-degeneracy splitting detected for the $^7F_{0-2}$ levels, the observation of this same number of local-field split components over the entire range of excitation wavelength used, and the $^5D_0 \rightarrow {}^7F_0$ full width at half maximum intensity ($19-31\,cm^{-1}$), indicate that the local environment of Eu^{3+} consist of a continuous distribution of closely similar low-symmetry network sites. In both $U(2000)_n Eu(CF_3SO_3)_3$ and $U(2000)_n EuBr_3$ hybrids the Eu^{3+} cations are coordinated by the carbonyl groups of the urea moieties. However, for the former family of xerogels the coordination between the cations and the oxygen ligands of the SO_3 end group of the triflate anions induces a rather high local site symmetry hybrids, when compared to the $U(2000)_n EuBr_3$ and the $POE_n EuBr_3$ materials.

In accordance with the local-field splitting of the $^7F_{1,2}$ levels, the coordination number determined by EXAFS, and the redshift of the $^5D_0 \rightarrow {}^7F_0$ transition (with respect to the value calculated for the gaseous case) a possible local charge distribution around the cations is suggested for the $U(2000)_{80} Eu(CF_3SO_3)_3$ hybrid, in which there are four available carbonyl oxygens for each incorporated europium ion. The Eu^{3+} first coordination shell is depicted as being formed by four carbonyl oxygens, five (or four) oxygen atoms from the SO_3 end groups of the triflate anions and two (or three) water molecules.

The tendency of the first ligands to bond covalently to the metal cations are discussed in terms of the energy of the intraconfigurational charge-transfer transitions, of the redshift of the $^5D_0 \rightarrow {}^7F_0$ line, and of the hypersensitive ratio between the $^5D_0 \rightarrow {}^7F_2$ and $^5D_0 \rightarrow {}^7F_1$ transitions. This analysis points out a rather low covalency nature of the Eu^{3+} first coordination shell in the ureasils xerogels, comparing to the case of analogous polymer electrolytes modified by europium bromide. On the other hand, the maximum I_{0-2}/I_{0-1} value and the minimum CTT energy observed for $U(2000)_{80} Eu(CF_3SO_3)_3$ suggest a greater degree of covalency for the Eu^{3+} first coordination shell. The existence in this salt concentration of four available carbonyl oxygens per each incorporated europium ion is certainly the main reason which account for the greater tendency of the first ligands to bond covalently to the metal ion in that salt concentration.

The barycenters of the emission transition energies for $U(2000)_n Eu(CF_3SO_3)_3$ were modeled by a free ion Hamiltonian written in terms of the electrostatic and spin-orbit parameters, F^2 and ζ. A microscopic model was used for defining a mean radius for the first coordination shell of Eu^{3+} in the ureasils, in terms of the empirically determined free ion parameters $F^{2,4,6}$ and ζ. The results obtained for the average Eu^{3+} first neighbors distance, approximately 2.4 Å for $40 \geqslant n \geqslant 90$ and 2.6 and 2.5 Å for $n=30$ and 20, respectively, are in very good agreement with the values calculated from EXAFS measurements.

ACKNOWLEDGMENTS

L.D.C. wishes to thank A. L. L. Videira (Physics Department of Évora University, Portugal), O. L. Malta (Fundamental Chemistry Department of Pernambuco Federal University, PE-Brazil), and H. F. Brito (Chemistry Institute of S. Paulo University, SP-Brazil) for fruitful discussions and comments. The authors also wish to express their gratitude to the staff of the National Laboratory of Synchrotron Light, LNLS, Campinas-SP Brazil. The financial support from FCT (PRAXIS/P/CTM/13175/98, 2/2.1/FIS/302/94, and BD/18404/98), ICCTI, and FAPESP is gratefully acknowledged.

*Author to whom correspondence should be addressed.

[1] See, for instance, *Polymer Electrolyte Reviews—1 and 2*, edited by J. R. MacCallum and C. A. Vincent (Elsevier Applied Science, London, 1987 and 1989).

[2] F. M. Gray, *Solid Polymer Electrolytes: Fundamentals and Technological Applications*, (VCH, New York, 1991); *Solid State Electrochemistry*, edited by P. G. Bruce (Cambridge University Press, 1995); F. M. Gray, *Polymer Electrolytes*, (RSC Materials Monographs, The Royal Society of Chemistry, London, 1997).

[3] M. Armand, Solid State Ionics **69**, 309 (1994); D. Baril, C. Michot, and M. Armand, *ibid.* **94**, 35 (1997).

[4] P. Lightfoot, M. A. Mehta, and P. G. Bruce, Science **262**, 883

(1993); P. Lightfoot, J. L. Nowinski, and P. G. Bruce, J. Am. Chem. Soc. **116**, 7469 (1994); P. G. Bruce, Electrochim. Acta **40**, 2077 (1995).

[5] S. Yoon, K. Ichikawa, W. J. MacKnight, and S. L. Hsu, Macromolecules **28**, 4278 (1995).

[6] A. Bernson, J. Lindgren, W. Huang, and R. Frech, Polymer **36**, 4471 (1995).

[7] B. L. Papke, M. A. Ratner, and D. F. Shriver, J. Electrochem. Soc. **129**, 1434 (1982); **129**, 1694 (1982).

[8] W. Huang, R. Frech, and R. A. Wheeler, J. Phys. Chem. **98**, 100 (1994), and references therein.

[9] R. Frech and W. Huang, Macromolecules **28**, 1246 (1995).

[10] A. Brodin, B. Mattson, K. Nilsson, L. M. Torell, and J. Hamara, Solid State Ionics **85**, 111 (1996).

[11] A. Ferry, M. M. Doeff, and L. C. De Jonghe, J. Electrochem. Soc. **145**, 1586 (1998).

[12] A. Ferry, J. Phys. Chem. B **101**, 150 (1997).

[13] P. G. Bruce, F. Krok, J. L. Nowinski, F. M. Gray, and C. A. Vincent, Mater. Sci. Forum **42**, 193 (1989); R. Huq and G. C. Farrington, in *Second International Symposium on Polymer Electrolytes*, edited by B. Scrosati (Elsevier Applied Science, London, 1990), p. 281; A. S. Reis Machado and L. Alcácer, *ibid.*, p. 283; C. J. Silva and M. J. Smith, Solid State Ionics **58**, 269 (1992).

[14] L. D. Carlos, M. Assunção, T. M. Abrantes, and L. Alcácer, in *Solid State Ionics III*, edited by G.-A. Nazri, J.-M. Tarrascon, and M. Armand, MRS Symposia Proceedings No. 293 (Material Research Society, Pittsburgh, 1993), p. 117.

[15] L. D. Carlos and A. L. L. Videira, Phys. Rev. B **49**, 11 721 (1994).

[16] L. D. Carlos and A. L. L. Videira, J. Chem. Phys. **101**, 8827 (1994).

[17] A. Brodin, B. Mattsson, and L. M. Torell, J. Chem. Phys. **101**, 4621 (1994).

[18] L. D. Carlos, M. Assunção, and L. Alcácer, J. Mater. Res. **10**, 202 (1995).

[19] L. D. Carlos, A. L. L. Videira, M. Assunção, and L. Alcácer, Electrochim. Acta **40**, 2143 (1995).

[20] L. D. Carlos and M. Assunção, J. Mater. Res. **11**, 2104 (1996).

[21] L. D. Carlos, Solid State Ionics **85**, 181 (1996).

[22] V. Di Noto, M. Bettinelli, M. Furlani, S. Lavina, and M. Vidali, Macromol. Chem. Phys. **197**, 257 (1996).

[23] A. L. L. Videira and L. D. Carlos, J. Chem. Phys. **105**, 8878 (1996); L. D. Carlos and A. L. L. Videira, Chem. Phys. Lett. **57**, 264 (1997).

[24] A. Ferry, M. Furlani, A. Franke, P. Jacobsson, and B.-E. Mellander, J. Chem. Phys. **109**, 2921 (1998); M. Furlani, A. Ferry, A. Franke, P. Jacobsson, and B.-E. Mellander, Solid State Ionics **113-115**, 129 (1998).

[25] See, for instance, H. Ohno and H. Yoshihara, Solid State Ionics **80**, 251 (1995); M. Makaigawa and H. Ohno, J. Electroanal. Chem. **452**, 141 (1998).

[26] M. Bredol, U. Kynast, and C. Ronda, Adv. Mater. **3**, 361 (1991); V. Alexander, Chem. Rev. **95**, 273 (1995).

[27] N. Sabbatini, M. Guardigli, and J.-M. Lehn, Coord. Chem. Rev. **123**, 201 (1993); N. Sabbatini, M. Guardigli, I. Manet, R. Ungaro, A. Casnati, R. Ziessel, Z. Ulrich, Z. Asfari, and J.-M. Lehn, Pure Appl. Chem. **67**, 135 (1995).

[28] W. Gorecki, M. Jeannin, E. Beloritzky, C. Roux, and M. Armand, J. Phys.: Condens. Matter **7**, 6823 (1995); A. Bakker, S. P. Gejji, J. Lindgren, K. Hermansson, and M. M. Probst, Polymer **36**, 4371 (1995).

[29] L. D. Carlos, V. De Zea Bermudez, M. C. Duarte, M. M. Silva, C. J. Silva, M. J. Smith, M. Assunção, and L. Alcácer, in *Physics and Chemistry of Luminescent Materials VI*, edited by C. Ronda and T. Welker (Electrochemical Soc. Proc., San Francisco, 1998), Vol. 97-29, p. 352.

[30] V. De Zea Bermudez, L. D. Carlos, M. C. Duarte, M. M. Silva, C. J. Silva, M. J. Smith, M. Assunção, and L. Alcácer, J. Alloys Compd. **275-277**, 21 (1998).

[31] S. J. L Ribeiro, K. Dahmouche, C. A. Ribeiro, C. V. Santilli, and S. H. J. Pulcinelli, J. Sol-Gel Sci. Technol. **13**, 427 (1998).

[32] L. D. Carlos, V. De Zea Bermudez, and R. A. Sá Ferreira, J. Non-Cryst. Solids **247**, 203 (1999).

[33] A. C. Franville, D. Zambon, R. Mahiou, S. Chou, Y. Troin, and J. C. Cousseins, J. Alloys Compd. **275-277**, 831 (1998).

[34] See, for instance, *Sol-gel Science and Technology*, edited by E. J. A. Pope, S. Sakka, and L. S. Klein (The American Ceramic Society, Westerville, 1995), Vol. 55; *Sol-gel Science: The Physics and Chemistry of Sol-Gel Processing*, edited by C. J. Brinker and G. W. Scherer (Academic Press, San Diego, 1990); H. Schmidt, in *Spectroscopy and Applications of Sol-Gel Glasses*, edited by R. Reisfeld and C. K. Jørgensen (Springer-Verlag, Berlin, 1991), p. 117.

[35] R. Reisfeld, in *Sol-Gel Science and Technology*, edited by M. A. Aegerter, J. M. Jafelicci, J. F. Souza, and E. D. Zanotto (Word Scientific, Singapore, 1989), p. 323; R. Reisfeld and C. K. Jørgensen, in *Chemistry, Spectroscopy and Applications of Sol-Gel Glasses*, edited by R. Reisfeld and C. K. Jørgensen (Springer-Verlag, Berlin, 1991), p. 207.

[36] R. Reisfeld, J. Non-Cryst. Solids **121**, 254 (1990); R. Campostrini, G. Carturan, M. Ferrari, M. Montagna, and O. Pilla, J. Mater. Res. **7**, 745 (1992); V. C. Costa, M. J. Lochhead, and K. L. Bray, Chem. Mater. **8**, 783 (1996).

[37] T. Jin, S. Tsutsumi, K. Machida, and G. Adachi, J. Electrochem. Soc. **143**, 3333 (1996); T. Jin, S. Inoue, S. Tsutsumi, and K. Machida, J. Non-Cryst. Solids **223**, 123 (1998).

[38] M. A. Zaitoun, T. Kim, and C. T. Lin, J. Phys. Chem. B **102**, 1122 (1998).

[39] P. Judeinstein and C. Sanchez, J. Mater. Chem. **6**, 511 (1996).

[40] W. H. Green, K. P. Le, J. Grey, T. T. Au, and M. J. Sailor, Science **276**, 1826 (1997).

[41] M. J. García, M. A. Mondragón, C. S. Téllez, A. Campero, and V. M. Castaño, Mater. Chem. Phys. **15**, 41 (1995).

[42] L. D. Carlos, V. De Zea Bermudez, R. A. Sá Ferreira, L. Marques, and M. Assunção, Chem. Mater. **11**, 581 (1999).

[43] R. A. Sá Ferreira, V. De Zea Bermudez, and L. D. Carlos, Thin Solid Films **343**, 470 (1999).

[44] C.-I. Chao and S.-A. Chen, Appl. Phys. Lett. **73**, 426 (1998); S. Tasch, E. J. W. List, O. Ekstrm, W. Graupner, G. Leising, P. Schlichting, U. Rohr, Y. Geerts, U. Scherf, and K. Mllen, *ibid.* **71**, 2883 (1997).

[45] J. Kido, M. Kimura, and K. Nagai, Science **267**, 1332 (1995).

[46] F. Hide, M. A. Díaz-García, B. J. Schwartz, M. R. Andersson, Q. Pei, and A. J. Heeger, Science **273**, 1833 (1996); F. Hide, P. Kozody, S. P. DenBaars, and A. J. Heeger, Appl. Phys. Lett. **70**, 2664 (1997).

[47] S. Taboada, A. de Andres, J. E. Munoz-Santiuste, C. Prieto, J. L. Martinez, and A. Criado, Phys. Rev. B **50**, 9157 (1994); J. A. Solera, J. García, and M. G. Proietti, *ibid.* **51**, 2678 (1995).

[48] S. L. Suib, R. P. Zerger, G. D. Stucky, T. I. Morrison, and G. K.

Shenoy, J. Chem. Phys. **80**, 2203 (1984).
[49] V. De Zea Bermudez, L. D. Carlos, and L. Alcácer, Chem. Mater. **11**, 569 (1999).
[50] M. Armand, C. J. Poinsignon, J.-Y. Sanchez, and V. De Zea Bermudez, French Patent **91**, 11 349 (1991); V. De Zea Bermudez, D. Baril, J.-Y. Sanchez, M. Armand, and C. J. Poinsignon, Proc. SPIE **1728**, 180 (1992).
[51] B. K. Teo, *Exafs: Basic Principles and Data Analysis* (Springer-Verlag, Berlin, 1985).
[52] A. Michalowicz (unpublished).
[53] V. V. Ovsyankin, in *Spectroscopy of Solids Containing Rare Earth Ions*, edited by A. A. Kaplyanskii and R. M. MacFarlane (Elsevier Science Publishers, Amsterdam, 1987), p. 371.
[54] E. W. J. L. Oomen and A. M. A. van Dongen, J. Non-Cryst. Solids **111**, 205 (1989).
[55] M. S. Brandt, H. D. Fuchs, M. Stutzmann, J. Weber, and M. Cardona, Solid State Commun. **81**, 307 (1992); M. Stutzmann, M. S. Brandt, M. Rosenbauer, J. Weber, and H. D. Fuchs, Phys. Rev. B **47**, 4806 (1993).
[56] K. Takeda and K. Shiraishi, Phys. Rev. B **39**, 11 028 (1989); H. Tachibana, M. Matsumoto, Y. Tokura, Y. Moritomo, A. Yamaguchi, S. Koshihara, R. D. Miller, and S. Abe, *ibid.* **47**, 4363 (1993); Y. Kanemitsu, K. Susuki, S. Kyushin, and H. Matsumoto, *ibid.* **51**, 13 103 (1995).
[57] A. G. Cullis, L. T. Canham, and P. D. J. Calcott, J. Appl. Phys. **82**, 909 (1997); A. Pifferi, P. Taroni, A. Torricelli, G. Valentini, P. Mutti, G. Ghislotti, and L. Zanghieri, Appl. Phys. Lett. **70**, 348 (1997).
[58] O. L. Malta, M. A. Couto dos Santos, L. C. Thompson, and N. K. Ito, J. Lumin. **69**, 77 (1996); O. L. Malta, H. F. Brito, J. F. S. Menezes, F. R. Gonçalves e Silva, S. Alves, Jr., F. S. Farias, Jr., and A. V. M. Andrade, *ibid.* **75**, 255 (1997).
[59] V. De Zea Bermudez, L. D. Carlos, and A. P. Passos de Almeida (unpublished).
[60] S. T. Frey and W. De W. Horrocks, Jr., Inorg. Chim. Acta **229**, 383 (1995).
[61] R. Reisfeld and C. K. Jørgensen, *Lasers and Excited States of Rare-Earths* (Springer-Verlag, Berlin, 1987), Chap. 3.
[62] R. Reisfeld, E. Greenberg, R. N. Brown, M. G. Drexhage, and C. K. Jørgensen, Chem. Phys. Lett. **95**, 91 (1983).
[63] See, for example, G. S. Ofelt, J. Chem. Phys. **38**, 2171 (1963).
[64] M. Zahir, R. Olazcuaga, C. Parent, G. Le Flem, and P. Hagenmuller, J. Non-Cryst. Solids **69**, 221 (1985).
[65] C. A. Morrison, J. Chem. Phys. **72**, 1001 (1980).
[66] K. C. A. Mishra, J. K. Berkowitz, K. H. Johnson, and P. C. Schmidt, Phys. Rev. B **45**, 10 902 (1992).
[67] C. A. Morrison, in *Angular Momentum Theory Applied to Interactions in Solids*, edited by G. Berthier *et al.*, Lecture Notes in Chemistry Vol. 47 (Springer-Verlag, Berlin, 1988).